Seeded optical parametric generation in $CdSiP_2$ pumped by a nanosecond pulsed, MHz repetition rate Raman fiber amplifier at 1.24 µm

Robert T. Murray[a*], Anita M. Chandran[a], Ronan A. Battle[a], Timothy H. Runcorn[a], Peter. G. Schunemann[b], Kevin T. Zawilski[b], Shekhar Guha[c], and James R. Taylor[a]

[a]Femtosecond Optics Group, Department of Physics, Imperial College London, Prince Consort Road, London SW7 2BW, UK
[b]BAE Systems, Inc., MER15-1813, P.O. Box 868, Nashua, New Hampshire 03061-0868, USA
[c]Air Force Research Laboratory, Materials and Manufacturing Directorate, Wright Patterson Air Force Base, Ohio 45433, USA

ABSTRACT

We report a $CdSiP_2$ (CSP) based seeded optical parametric generator (OPG), emitting sub-nanosecond duration, 3 MHz repetition rate, wavelength tunable mid-infrared (MIR) light at 4.2–4.6 µm. We generate up to 0.25 W at 4.2 µm with a total pump conversion efficiency of 42%. The OPG is pumped by a 1.24 µm Raman fiber amplifier system. This is the first demonstration of pumping CSP with a Raman fiber source in this region, and we show that Raman fiber sources in the near-infrared (NIR) are ideal pump sources for non-critically phasematched (NCPM) CSP devices. Pumping CSP at 1.24 µm permits the use of NCPM whilst decreasing the negative effects of both two-photon absorption and linear absorption losses, when compared to conventional 1 µm pumping. This offers a potential advantage for MIR power scaling of CSP parametric devices due to a reduced thermal load in the crystal from residual pump absorption. The OPG is seeded with a continuous-wave fiber supercontinuum source emitting radiation in the 1.7 µm region, to lower the threshold pump intensity required for efficient conversion. NCPM and temperature tuning of the crystal allow for simple wavelength tuning of the idler radiation. We report on laser damage induced by elevated crystal temperatures, which we propose is linked to the decrease in CSP bandgap energy with increasing temperature.

Keywords: Optical parametric generation; Raman fiber amplifiers; Chalcopyrites; $CdSiP_2$; Nonlinear conversion; Fiber amplifiers; Mid-infrared

1. INTRODUCTION

There are a wide range of applications in science, industry and defense requiring high brightness, coherent sources of radiation in the 3–5 µm MIR wavelength region.[1–3] Directly emitting sources in this region are scarce, or lack the required performance for many applications, with viable sources limited to MIR fiber lasers, quantum cascade lasers and Cr/Fe-doped II-VI chalcogenide solid-state lasers.[4–6] Such sources have matured in both power and spectral coverage in recent years. However, they still cannot match optical parametric devices based on nonlinear three-wave mixing processes (χ^2), in terms of the pulse durations and pulse energies, repetition rates and wavelength ranges they can produce.

The standard approach to generating light in the 3–5 µm band with optical parametric wavelength conversion is to employ well-established laser technology, typically in the 1 µm band, such as those based on the Nd^{3+} or Yb^{3+} active ions, and upconvert this light to the MIR with a suitable nonlinear crystal. Lasers based on Nd^{3+}/Yb^{3+} are available with both high peak powers (MWs) and average powers (kWs), so provided a suitable nonlinear crystal is available for the wavelength conversion this is a viable route to high power MIR sources. The most commonly used crystals for generating light in the 3–5 µm band are those from the oxide family, typically either periodically poled lithium tantalate (PPLT) or periodically poled lithium niobate (PPLN).[7] However, the

*Further author information – Contact email: robert.murray10@imperial.ac.uk

oxides become increasingly absorptive above 4 µm due to the onset of the infrared (IR) absorption edge, which quickly leads to thermal lensing, thermal dephasing, and ultimately, crystal damage when operating at higher average power levels.[8]

If light at wavelengths > 4 µm is required, the gold-standard approach is to employ $ZnGeP_2$ (ZGP) as the nonlinear conversion medium, a chalcopyrite crystal which has both an exceptionally high nonlinear coefficient (75 pm/V) and a large thermal conductivity (35 W/mK).[9] Due to the relatively small bandgap energy of ZGP, however, pump wavelengths of ≥ 1.9 µm are required to avoid excessive pump light absorption and its associated problems. There are also a lack of phasematching options at wavelengths shorter than 1.9 µm in ZGP.

$CdSiP_2$ (CSP), offers an exciting alternative to ZGP. CSP is an optical semiconductor with a large bandgap energy of 2.45 eV (506 nm) which permits pumping down to the 1 µm band, whilst avoiding issues with two-photon absorption. CSP also remains transparent up to 6.5 µm.[10] CSP is exceptionally nonlinear, having a $d_{36} = 84.5$ pm/V at 4.46 µm;[11] this is the largest nonlinear coefficient of any new phase-matchable inorganic crystal discovered in the last four decades.[9] In addition, CSP permits a wide range of phasematching options for pump sources across the 1–2 µm region, both in critical and non-critical configurations.

The wide range of phasematching options CSP offers has been explored extensively in recent years. 1.5 µm and 1.9 µm pumping is particularly attractive as it enables the generation of MIR light in the 3–5 µm region.[12,13] Due to the relatively high (in wavelength) degeneracy point of these 1.5/1.9 µm pumped devices, in particular those pumped at 1.9 µm, the total pump conversion to the MIR band can be very high, on the order of $> 60\%$.[14] However, phasematching at these pump wavelengths is achieved critically, which places tighter restrictions on the angular acceptance bandwidths and can lead to degradations in output beam quality due to walk-off. The majority of the work undertaken with CSP over the last decade has concentrated instead on 1 µm pumping.[15–17] At this pump wavelength, non-critical phasematching (NCPM) can be employed and simple wavelength tuning of the generated signal and idler waves is possible through crystal temperature adjustment. The phasematching is such that the MIR idler radiation falls within the 6-7 µm region. This coincides with strong absorption bands of both water and the amide proteins, which led to interest in developing 1 µm pumped CSP based sources for surgical applications.[18] However, when operating so close to the transmission edge of CSP with 1 µm pumping, issues with both two-photon absorption (TPA) and residual linear absorption can arise, limiting the power scaling potential and increasing the susceptibility of CSP to laser induced damage.[19,20]

In this work, we investigate the pumping of CSP at wavelengths beyond the conventional 1 µm band, whilst still employing NCPM. The potential of this scheme was first demonstrated by Marchev and et al.[17] They employed a 1 kHz repetition rate, 150 ps duration Raman shifted source at 1.2 µm, generating MIR radiation at 4.64 µm. We instead employ a 1.24 µm Raman fiber amplifier system at MHz repetition rates, to explore the power scaling potential of this architecture. We also demonstrate, for the first time with a 1.2 µm pump, wide idler wavelength tuning of a NCPM based CSP device, generating tunable MIR radiation from 4.2–4.6 µm. The pairing of Raman fiber sources and NCPM in CSP represents an exciting new architecture for generating high power, widely tunable radiation in the difficult to reach 4–5 µm band. In the remainder of this article, we discuss the following: in Section 2 we discuss NCPM in CSP; in Section 3 we describe the pulsed Raman fiber amplifier systems we have developed in our group in recent years, and that make ideal pump sources for NCPM CSP devices; in Section 4 we present our results on seeded optical parametric generation (OPG) in CSP; in Section 5 we summarize with conclusions and an outlook on future work in this area.

2. NON-CRITICAL PHASEMATCHING IN CSP

Figure 1 (a) shows the phasematched signal and idler wavelengths for pump wavelengths in the 1–1.4 µm regions in a 90° cut, type-I (oo-e) non-critical interaction in CSP. These were calculated using the most up-to-date temperature dependent Sellmeier equations for CSP.[24] As can be seen, pumping in the region of well-developed laser technology around 1 µm generates idler radiation in the 6–7 µm band. By increasing the pump wavelength from 1 µm, the generated idler radiation will correspondingly shift down in wavelength into the important 3–5 µm band. This will also result in lower residual absorption, as indicated by the dashed-dotted line, which should help with reducing the effects of laser damage and thermal lensing issues in the CSP. A shift away from the bandgap edge will also result in a drop in the TPA coefficient, important for the same reasons. Finally, a longer pump

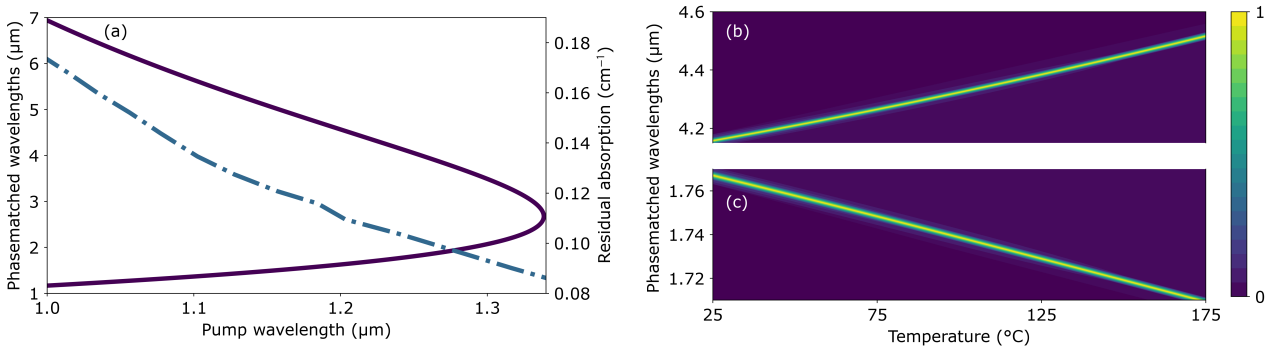

Figure 1. (a) Phasematched signal and idler wavelengths for non-critical 90° type-I (oo-e) in CSP, purple solid line. Residual absorption of CSP as a function of pump wavelength, dashed-dotted blue line. (b) Phasematched idler and signal (c) wavelengths against crystal temperature, colorbar indicates the theoretical conversion efficiency.

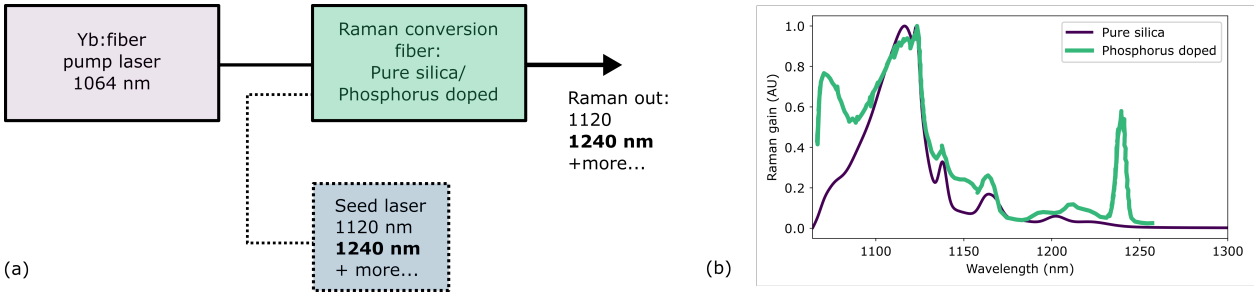

Figure 2. (a) Raman fiber amplifier schematic. (b) Raman gain curves for a pure-silica core optical fiber, calculated using the multiple vibration mode model,[21] and a phosphorus doped core fiber.[22,23]

wavelength also reduces the quantum defect between the pump and idler radiation, leading to greater pump to MIR conversion efficiencies. One advantage of NCPM compared to critical phasematching (CPM), is the ease with which output wavelength tuning can be achieved. Figures 1 (b) and (c) highlight this, demonstrating the signal and idler wavelength tunability possible through temperature tuning the CSP crystal.

3. RAMAN FIBER AMPLIFIERS

In this section, we will first briefly introduce stimulated Raman scattering (SRS) in optical fibers (3.1), with an emphasis on producing different wavelengths suitable for NCPM CSP based devices, before describing an exemplar 1.24 μm Raman fiber amplifier used for the OPG experiments in this work (3.2).

3.1 Stimulated Raman scattering in optical fibers

Spontaneous Raman scattering describes the inelastic scattering of light from a medium. In the scattering process, incident photons stimulate lattice vibrations through which energy is lost, in the form of phonons. The loss in photon energy causes a corresponding shift in frequency of the photon. In the spontaneous Raman case, the fraction of light scattered is very low, on the order of 10^{-6}. This process becomes much more efficient when a Stokes wave at the correct frequency shift is also present in the material (or enough light builds up from the spontaneous scattering process). When the Stokes wave grows exponentially in proportion to the pump intensity, the process becomes known as stimulated Raman scattering (SRS).

SRS can very efficiently transfer energy from the pump light to the Stokes wave. In optical fibers, conversion efficiencies of >90% from the pump to the first Stokes wave are readily achievable.[25,26] The frequency shift from the pump to the Stokes wave is set by the composition of the material in use. In standard silica optical fibres (pure-silica), the main Raman gain peak is centred around 13 THz, shown in Fig. 2 (b). In fibers doped with phosphorus (phosphorus doped), there is a secondary peak at around 40 THz, also shown in Fig. 2 (b). This

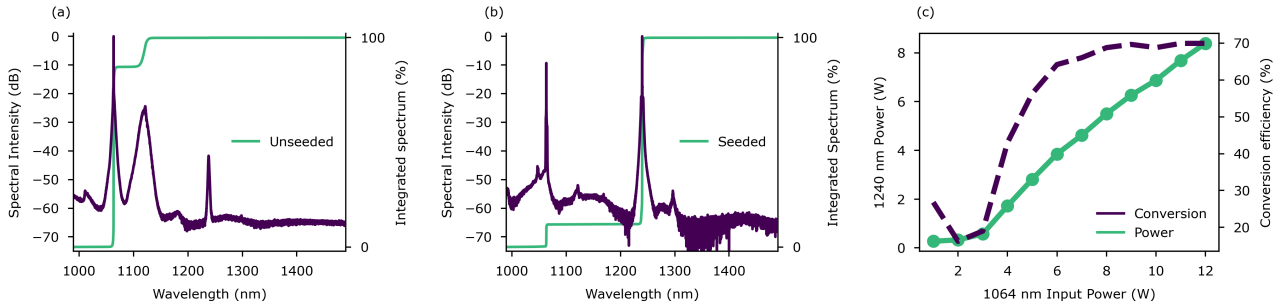

Figure 3. 1.24 µm Raman fiber amplifier characteristics. (a) Output spectrum with no seeding. (b) Output spectrum with seeding. (c) 1.24 µm output power and conversion efficiency as a function of 1.06 µm input pump power.

larger frequency shift can be exploited to develop light sources in the 1.2 µm region, ideal for pumping NCPM CSP devices.

A general scheme of a Raman fiber amplifier system is shown in Fig. 2 (a). A Yb:fiber pump laser operating at 1.064 µm is typically used to pump a Raman conversion stage, which could be a standard pure silica fiber or a phosphorus doped silica fiber. By seeding the Raman conversion stage with an appropriate seed laser for the given fiber composition, it is possible to create arbitrary wavelength sources throughout the NIR. The output wavelength of the Raman fiber amplifier will be set by the starting pump wavelength, the choice of seed wavelength and the type of Raman conversion employed. It is also possible to cascade multiple Raman shifts, to shift the pump wavelength further into the NIR. In recent years, our group has demonstrated such sources at 1.12 µm, 1.18 µm and 1.24 µm, which were all then subsequently frequency doubled for biophotonics imaging applications.[27–31] However, as we demonstrate in this work, NIR Raman fiber systems are also highly suitable for upconversion to the MIR.

3.2 An exemplar Raman fiber amplifier operating at 1.24 µm

In this work, we employ a 1.24 µm pulsed Raman fiber amplifier, similar to our previous work.[31] A pulsed Yb:fiber master oscillator power amplifier (MOPA) system centered at 1.064 µm is used as the pump laser. The seed oscillator is a gain-switched laser diode emitting pulses that are both duration and repetition rate tunable, from 0.05–2 ns and 1–20 MHz. The pulses are amplified in two polarization-maintaining (PM) Yb:fiber amplifiers, with average power levels of up to 20 W available.

This pump light at 1.064 µm is then coupled into a 5 m length of PM phosphosilicate fiber (FORC P-SM-5-PM). Phosphorus doped fiber was employed over pure silica fiber in order to exploit the larger 40 THz shift (see Fig. 2 (b)) and generate light at 1.24 µm. The length of the PM phosphosilicate fiber was carefully optimized to enable the maximum conversion into the 1.24 µm Raman peak, whilst minimizing the onset of competing nonlinear effects in the fiber (self/cross phase modulation, four-wave mixing), and the cascade to higher order Raman Stokes shifts.

The output spectra of the phosphosilicate Raman fiber amplifier are shown in Figs 3 (a) and (b), for the unseeded and seeded cases respectively, see Fig. 2 (a) for details of the setup. The green line is the integrated spectral content, and indicates where the power is distributed in the spectrum. In the unseeded case, Fig. 3 (a), the 13 THz Raman shift at 1.12 µm and the 40 THz Raman shift at 1.24 µm are both evident. However, as shown by the integrated spectral content the majority of the pump power has not been converted to either of the Raman shifts. To improve the conversion, we seed the 40 THz Raman shift with a fiber Bragg grating stabilized laser diode operating at 1.24 µm. The seed diode provides up to 300 mW of output power, but the Raman amplifier is saturated at seed powers as low as 1 mW. As can be seen in Fig. 3 (b), the effect of seeding the 1.24 µm Raman line is impressive. Not only is the 1.12 µm Raman Stokes line almost completely suppressed, but the majority of the integrated spectral power now also lies at 1.24 µm.

Figure 3 (c) shows the 1.24 µm output power of the amplifier as a function of 1.06 µm input power. At a maximum input power of 12 W, we generate greater than 8 W of power at 1.24 µm. The amplifier is highly

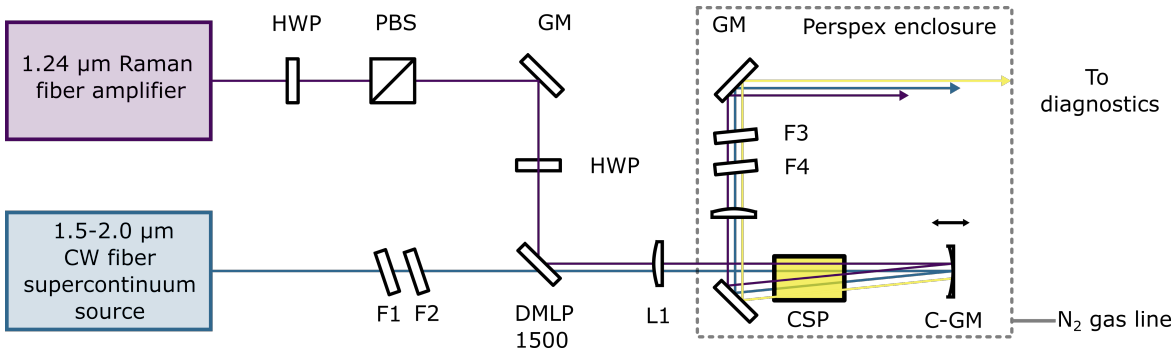

Figure 4. Experimental setup for seeded optical parametric in CSP. The 1.24 µm Raman fiber amplifier acts as the pump with a continuous wave fiber supercontinuum source providing the seed signal, pumping the CSP crystal in a double pass configuration to generate idler radiation in the 4.2–4.6 µm band. The acronyms used in the diagram are defined in the main body text.

efficient, with the conversion efficiency reaching 70% at the highest input pump powers. When we account for fiber coupling losses, the internal conversion efficiency of the amplifier exceeds 80%, close to the quantum defect limited conversion of 85% (1.06 µm to 1.24 µm). As the Raman conversion fiber used is single mode at 1.24 µm, the generated light displays excellent diffraction limited beam quality with an $M^2 = 1.01$, and is linearly polarized with a polarization extinction ratio of 19 dB. Such a source is ideal for nonlinear wavelength conversion in CSP to the MIR. For further details on the 1.24 µm source, the reader is directed to Ref.[31]

4. SEEDED OPTICAL PARAMETRIC GENERATION IN CSP

In this section, we first describe in detail the experimental setup used for seeded OPG in CSP (4.1) before presenting our results on the OPG itself (4.2).

4.1 OPG setup

The 1.24 µm Raman amplifier detailed in Section 3.2 is then used for seeded optical parametric generation in CSP, as shown in Fig. 4. The Raman amplifier acts as the pump laser, and for our experiments we employ a 3 MHz repetition rate, a pulse duration of 1 ns and an average power of up to 3 W, corresponding to a maximum pump pulse energy of 1 µJ. The pump pulse spectrum and temporal profile are shown in Figs. 5 (a) and (c), respectively. A polarizing beam-splitter (PBS) and half-wave plate (HWP) is used to control the 1.24 µm power delivered to the CSP crystal, and a second HWP is then used to align the pump polarization to the correct axis of the crystal. The pump light is focused into the CSP using a lens (L1) with a focal length of $f = 62.5$ mm. This results in a circular focused spot size of 60 µm (measured in air using a pyroelectric scanning slit profiler), corresponding to a maximum peak pump intensity of 54 MW/cm^2, which is slightly higher than the 1.06 µm CSP damage threshold value of 44 MW/cm^2.[20]

We employ a continuous-wave fiber supercontinuum source (CW-SC) as the seed signal, to initiate seeded OPG. The CW-SC source is based on a CW Er:fiber MOPA pumping a length of highly nonlinear fiber to create radiation in the 1.5-2.0 µm region.[32] Two interference filters are used (F1/F2) to spectrally select a portion of the CW-SC radiation centered around 1.7 µm, as shown in Fig. 5 (b). The central wavelength of this radiation can be shifted by adjusting the angular position of the filters F1 and F2. After filtering there is approximately 200 mW of power available to seed the OPG. Due to the non polarisation-maintaining nature of the fibers used in the CW-SC stage, the output light is unpolarized. The CW-SC is crucial in our system: it allows easy idler wavelength tuning due to the broadband nature of the seed radiation, and it lowers the pump intensity threshold for efficient OPG conversion. Also, owing to its CW nature, no synchronization is needed between the pump and signal. A double pass of the CSP crystal is also employed to lower the pump intensity threshold further. This lowering of the pump threshold is critical, owing to the susceptibility of CSP to laser induced damage, with recently reported values in the literature of 44 MW/cm^2 and 0.35 J/cm^2.[20] The values quoted here are

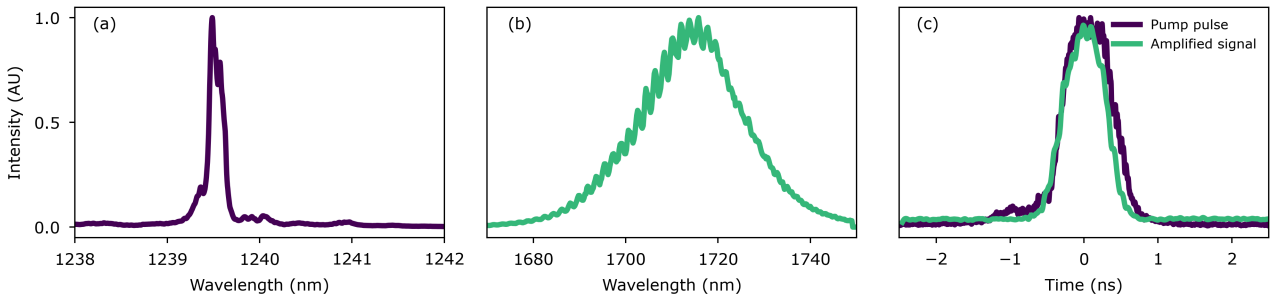

Figure 5. (a) Pump and (b) signal spectral characteristics. (c) Temporal characteristics of the pump and amplified signal pulses.

for a 1.06 µm pump wavelength. In this work we shift the pump wavelength to 1.24 µm and would expect a corresponding increase in the laser damage threshold.[19,20]

The pump and signal beams are combined using a dichroic mirror (DMLP1500) and overlapped at the focus of L1 with the aid of a pyroelectric scanning slit profiler. The CSP crystal used is 13 mm long, with a 3x6 mm^2 aperture. The crystal is cut at 90° for type-I (oo-e) NCPM, as discussed in Section 2. Both surfaces of the crystal are anti-reflection (AR) coated with a standard electron beam evaporation coating [LaserOptik GmbH], with a single pass transmission for the pump, signal and idler light of $T_p = 0.93$, T_s=0.91 and T_i=0.9, respectively. The crystal is mounted in a copper oven, which is tunable in temperature from 25–250°C. After the first pass through the crystal, the beams are refocused for a second pass back through the crystal using a curved gold mirror ($f = 50$ mm). The mirror is positioned at a distance $2f$ from the CSP crystal, such that the returning beams form a waist at the same longitudinal position and size as the outgoing waist. A slight angular offset is introduced to allow the returning beam to be picked off using a gold D-shaped mirror. A CaF_2 lens ($f = 50$ mm) is then used to re-collimate the output of the OPG, before interference filters F3/F4 can be employed to separate the generated pump/signal/idler radiation for further characterization. The entire OPG stage is also housed in a sealed perspex enclosure which can be purged with N_2 gas.

4.2 OPG results

Once the pump and signal beams are overlapped in the crystal, strong OPG is observed. The powers generated from the OPG, both signal, idler and combined (signal plus idler), as a function of incident pump power are shown in Fig. 6 (a). The pump average power is the power incident on the face of the crystal, and the generated signal and idler powers have been corrected for losses through the filtering optics and the uncoated CaF_2 lens. We generate > 0.25 W of power at 4.2 µm, with pump to idler conversion efficiencies of $> 10\%$. We generate over 1 W of total OPG output power, signal plus idler, at a total pump conversion efficiency of 42%, as shown in Fig. 6 (b). However, the conversion efficiency begins to roll-off at the highest pump powers. A chopper wheel is then used to reduce the duty cycle of the pump laser to 50% of its full power, to keep the same peak intensity in the crystal but decrease the thermal load, shown in Fig. 6 (c). The reduction of the thermal load on the crystal is found to make no measurable difference to the overall pump conversion efficiency, from which we deduce that the roll-off must be caused either by OPG saturation, and the onset of back-conversion, or nonlinear absorption of the pump light.

The system as described is currently operating at a fluence of 0.06 J/cm^2, which is well below the quoted fluence damage threshold of 0.35 J/cm^2 for CSP at 1.064 µm.[20] As the roll-off in conversion does not be appear to be linked to excessive average power, and corresponding absorption in the crystal, we propose further power scaling could be possible in this configuration. Increasing the pulse duration and corresponding pulse energy through an increase in average power, whilst keeping the peak intensity in the CSP the same, it could be possible to maintain the same conversion efficiency levels but increase the powers by a factor of ≈5. This is the subject of ongoing work.

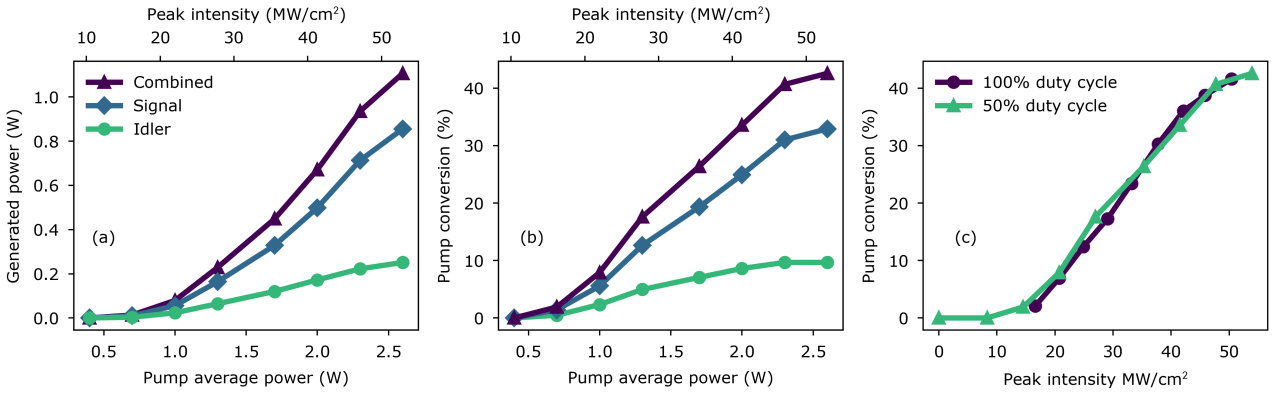

Figure 6. Output power characteristics of the CSP OPG. (a) Generated signal, idler and combined (signal plus idler) powers as a function of 1.24 µm pump power. (b) Corresponding conversion efficiencies for the OPG. (c) Pump conversion for different duty cycles of the pump laser, at 100% and 50% of the total average power load in the crystal, as a function of instantaneous peak power.

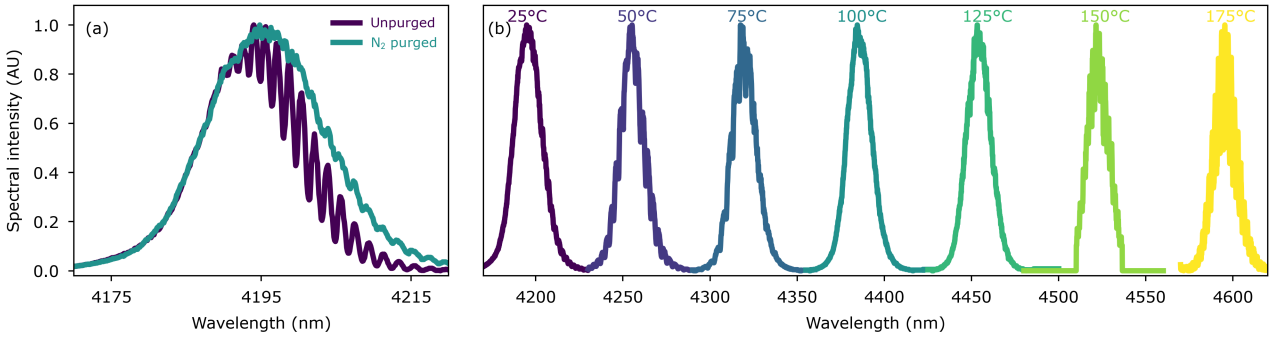

Figure 7. (a) Example idler spectrum with atmospheric carbon dioxide absorption evident (unpurged) and with absorption eliminated (purged - using N_2 gas). (b) Wide idler tuning possible through temperature tuning the CSP crystal.

The MIR idler spectrum output of the OPG is shown in Fig. 7 (a), when pumped with the pump and signal spectra shown in Fig. 5 (a) and (b). There are strong modulations in the idler spectrum, caused by absorption due to carbon dioxide in the laboratory atmosphere. By purging the OPG enclosure with N_2 gas, it is possible to almost completely eliminate the modulations present in the spectrum. As discussed in Section 2, NCPM allows for easy wavelength tuning of the OPG output by simple adjustment of the crystal temperature. By adjusting the crystal temperature from 25–175°C, the idler wavelength correspondingly tunes over the range 4.2–4.6 µm, as demonstrated in Fig. 7 (b). It is expected that further wavelength/temperature tuning should be possible, however, when the crystal was heated beyond 175°C bulk crystal damage was observed, in the form of a sudden decrease in output power and an accompanying degradation in beam quality. It is well known that an increase of the temperature of a semiconductor material results in a decrease in the bandgap energy. Thus, we propose that the bandgap energy of the CSP is decreasing with increasing temperature, leading to an increase in near-bandgap absorption and crystal heating, which above 175°C results in bulk crystal damage. In a recent study, Wei and co-workers showed that the absorption of CSP decreases at lower temperatures, which supports our hypothesis.[24] Increased absorption from free carriers is also thought to cause an increase in the susceptibility to laser induced damage at elevated temperatures. It is also observed in the experiments that the pump beam profile changes upon passing through the crystal at higher pump powers. Changing the crystal temperature at a constant pump power in the crystal also causes slight changes in the beam shape, as observed on a IR laser viewing card. Again, we believe this effect is due to changing absorption in the CSP with varying temperature. Ongoing work is aimed

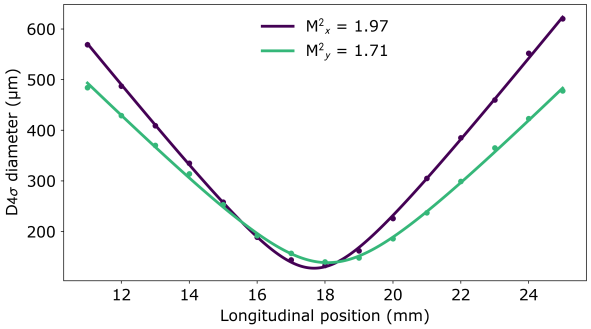

Figure 8. Idler beam caustics in the horizontal (x) and vertical (y) planes, with Gaussian fits overlaid.

at quantifying these effects more fully.

The idler beam at approximately 200 mW of power is then focused using an $f = 150$ mm lens, and the 4σ beam diameters are measured through the focused beam waist using a scanning slit beam profiler, shown in Fig. 8. Gaussian fits to the beam caustics are used to extract the M^2 values in the horizontal and vertical planes, with values of $M^2{}_x = 1.97$ and $M^2{}_y = 1.71$. The idler beam quality has degraded from the diffraction limited 1.24 μm pump beam, which is not unexpected given the issues with laser induced damage and thermally induced beam profile changes observed in the experiment. We also use an angular offset in the return pass in the double-pass OPG arrangement, which could also be degrading the beam quality of the idler.

5. CONCLUSIONS AND OUTLOOK

We have presented our work on Raman fiber amplifiers and their application to pumping NCPM based CSP OPGs. With a 1.24 μm Raman fiber amplifier as the pump, we generate widely tuneable MIR idler radiation in the 4.2–4.6 μm region, with idler powers exceeding 0.25 W and total pump conversion efficiencies of 42%. This is the first demonstration of MHz repetition rate pumping of CSP in the 1.2 μm region, and the first demonstration of such widely tunable idler radiation with this pump wavelength. The pairing of CSP and NIR Raman amplifiers in the 1.1–1.3 μm region represents an exciting new architecture with the potential to create high power, widely tunable radiation in the hard to access, but technologically important, 4–5 μm region of the MIR. Raman fiber sources are available at arbitrary wavelengths throughout the NIR, and CSP can be used to NCPM pump light in this region.

However, more work is needed to fully understand the potential of this architecture, in particular around the limitations of the linear and nonlinear absorption of CSP at Raman pump wavelengths throughout the NIR. We have found that operating CSP at elevated temperatures for prolonged periods may increase the susceptibility of the material to laser induced damage. This finding is particulary interesting as it places a potential upper limit on the wavelength tunability possible through temperature-tuned NCPM CSP based devices, which is one of the most attractive prospects of the NCPM architecture. Ongoing work is aimed at employing different Raman pump amplifier systems throughout the 1.1–1.3 μm region to demonstrate the full capability of this architecture. We are working to demonstrate further power scaling of the generated MIR light as proposed, and quantify further the different effects contributing to the degradation in the idler beam quality.

ACKNOWLEDGMENTS

The European Office of Aerospace Research and Development (FA9550-17-1-0194). This work has also been partially supported by the Functional Materials Division of the Materials and Manufacturing Directorate, Air Force Research Laboratory (AFRL/RXA) (FA8650-16-F-5418). RTM is supported by the Imperial College Research Fellowship scheme. THR is supported by the Royal Academy of Engineering under the Research Fellowship scheme. AMC and RAB acknowledge support from EPSRC funded studentships. The data used in this paper are openly avaialable at https://doi.org/10.5281/zenodo.4534738.

REFERENCES

[1] Kolev, V. Z., Duering, M. W., Luther-Davies, B., and Rode, A. V., "Compact high-power optical source for resonant infrared pulsed laser ablation and deposition of polymer materials," *Optics Express* **14**(25), 12302–12309 (2006).

[2] Sorokina, I. T. and Vodopyanov, K. L., [*Solid-State Mid-Infrared Laser Sources*], Springer (2003).

[3] Vodopyanov, K. L., [*Laser-based Mid-infrared Sources and Applications*], Wiley (2020).

[4] Jackson, S. D., "Towards High-Power Mid-Infrared Emission from a Fibre Laser," *Nature Photonics* **6**(7), 423–431 (2012).

[5] Yao, Y., Hoffman, A. J., and Gmachl, C. F., "Mid-infrared quantum cascade lasers," *Nature Photonics* **6**(7), 432–439 (2012).

[6] Mirov, S. B., Fedorov, V. V., Martyshkin, D., Moskalev, I. S., Mirov, M., and Vasilyev, S., "Progress in Mid-IR Lasers Based on Cr and Fe-Doped II–VI Chalcogenides," *IEEE Journal of Selected Topics in Quantum Electronics* **21**(1), 292–310 (2015).

[7] Murray, R. T., Runcorn, T. H., Guha, S., and Taylor, J. R., "High average power parametric wavelength conversion at 3.31-3.48 µm in MgO:PPLN," *Optics Express* **25**(6), 343–348 (2017).

[8] Lin, S. T., Lin, Y., Wang, T. D., and Huang, Y., "Thermal waveguide OPO," *Optics Express* **18**(2), 1323–1329 (2010).

[9] Schunemann, P. G., Zawilski, K. T., Pomeranz, L. A., Creeden, D. J., and Budni, P. A., "Advances in nonlinear optical crystals for mid-infrared coherent sources," *Journal of the Optical Society of America B* **33**(11), D36–D43 (2016).

[10] Zawilski, K. T., Schunemann, P. G., Pollak, T. C., Zelmon, D. E., Fernelius, N. C., and Hopkins, F. K., "Growth and characterization of large $CdSiP_2$ single crystals," *Journal of Crystal Growth* **312**(8), 1127–1132 (2010).

[11] Petrov, V., Noack, F., Tunchev, I., Schunemann, P. G., and Zawilski, K. T., "The nonlinear coefficient d_{36} of $CdSiP_2$," in [*Nonlinear Frequency Generation and Conversion: Materials, Devices, and Applications VIII*], 71970M, Proc. SPIE 7197 (2009).

[12] Pomeranz, L., McCarthy, J., Day, R., Zawilski, K. T., and Schunemann, P. G., "Efficient, 2–5 µm tunable $CdSiP_2$ optical parametric oscillator pumped by a laser source at 1.57 µm," *Optics Letters* **43**(1), 130–133 (2018).

[13] Cole, B., Goldberg, L., Zawilski, K. T., Pomeranz, L. A., Schunemann, P. G., and McCarthy, J. C., "Compact and efficient mid-IR OPO source pumped by a passively Q-switched Tm:YAP laser," *Optics Letters* **43**(5), 1099–1102 (2018).

[14] Cole, B., Goldberg, L., Zawilski, K. T., Pomeranz, L. A., Schunemann, P. G., and McCarthy, J. C., "Compact efficient Tm:YAP pumped mid-IR OPO," in [*Solid State Lasers XXVIII: Technology and Devices*], **10896**, 30 – 37, International Society for Optics and Photonics, SPIE (2019).

[15] Petrov, V., Schunemann, P. G., Zawilski, K. T., and Pollak, T. M., "Noncritical singly resonant optical parametric oscillator operation near 6.2 µm based on a $CdSiP_2$ crystal pumped at 1064 nm," *Optics Letters* **34**(16), 2399–2401 (2009).

[16] Kumar, S. C., Jelínek, M., Baudisch, M., Zawilski, K. T., Schunemann, P. G., Kubeček, V., Biegert, J., and Ebrahim-Zadeh, M., "Tunable, high-energy, mid-infrared, picosecond optical parametric generator based on $CdSiP_2$," *Optics Express* **20**(14), 15703–15709 (2012).

[17] Marchev, G., Pirzio, F., Piccoli, R., Agnesi, A., Reali, G., Schunemann, P. G., Zawilski, K. T., Tyazhev, A., and Petrov, V., "Narrow-bandwidth, mid-infrared, seeded optical parametric generation in 90° phase-matched $CdSiP_2$ crystal pumped by diffraction limited 500 ps pulses at 1064 nm," *Optics Letters* **37**(15), 3219–3221 (2012).

[18] Kumar, S. C., Schunemann, P. G., Zawilski, K. T., and Ebrahim-Zadeh, M., "Advances in ultrafast optical parametric sources for the mid-infrared based on $CdSiP_2$," *Journal of the Optical Society of America B* **33**(11), D44–D56 (2016).

[19] Hildenbrand, A., Kieleck, C., Tyazhev, A., Marchev, G., Stöppler, G., Eichhorn, M., Schunemann, P., and Petrov, V., "Laser damage studies of $CdSiP_2$ and $ZnGeP_2$ nonlinear crystals with nanosecond pulses at 1064 and 2090 nm," in [*Nonlinear Frequency Generation and Conversion: Materials, Devices, and Applications XIII*], **8964**, 162 – 169, SPIE (2014).

[20] Hildenbrand-Dhollande, A., Kieleck, C., Marchev, G., Schunemann, P. G., Zawilski, K. T., Petrov, V., and Eichhorn, M., "Laser-Induced Damage Study at 1.064 and 2.09 µm of High Optical Quality $CdSiP_2$ Crystal," in [*Advanced Solid State Lasers*], AM2A.8, Optical Society of America (2015).

[21] Hollenbeck, D. and Cantrell, C. D., "Multiple-vibrational-mode model for fiber-optic Raman gain spectrum and response function," *Journal of the Optical Society of America B* **19**(12), 2886–2892 (2002).

[22] Shibata, N., Horigudhi, M., and Edahiro, T., "Raman spectra of binary high-silica glasses and fibers containing GeO_2, P_2O_5 and B_2O_3," *Journal of Non-Crystalline Solids* **45**(1), 115–126 (1981).

[23] Plotnichenko, V., Sokolov, V., Koltashev, V., and Dianov, E., "On the structure of phosphosilicate glasses," *Journal of Non-Crystalline Solids* **306**(3), 209–226 (2002).

[24] Wei, J., Murray, J. M., Hopkins, F. K., Krein, D. M., Zawilski, K. T., Schunemann, P. G., and Guha, S., "Measurement of refractive indices of $CdSiP_2$ at temperatures from 90 to 450 K," *Optical Materials Express* **8**(2), 235–244 (2018).

[25] Lin, C., Cohen, L., Stolen, R., Tasker, G., and French, W., "Near-infrared sources in the 1–1.3 µm region by efficient stimulated Raman emission in glass fibers," *Optics Communications* **20**(3), 426–428 (1977).

[26] Dianov, E. M., "Advances in Raman fibers," *Journal of Lightwave Technology* **20**(8), 1457–1462 (2002).

[27] Runcorn, T. H., Murray, R. T., Kelleher, E. J. R., Popov, S. V., and Taylor, J. R., "Duration-tunable picosecond source at 560 nm with Watt-level average power," *Optics Letters* **40**(13), 3085–3088 (2015).

[28] Runcorn, T. H., Murray, R. T., Kelleher, E. J. R., and Taylor, J. R., "Watt-level Nanosecond 589 nm Source by SHG of a Cascaded Raman Amplifier," in [*Lasers Congress 2016 (ASSL, LSC, LAC)*], ATh1A.3 (2016).

[29] Runcorn, T. H., Murray, R. T., and Taylor, J. R., "Highly efficient nanosecond 560 nm source by SHG of a combined Yb-Raman fiber amplifier," *Optics Express* **26**(4), 4440–4447 (2018).

[30] Runcorn, T. H., Gorlitz, F., Murray, R. T., and Kelleher, E. J. R., "Visible Raman-shifted Fiber Lasers for Biophotonic Applications," *IEEE Journal of Selected Topics in Quantum Electronics* **24**(3) (2018).

[31] Chandran, A. M., Runcorn, T. H., Murray, R. T., and Taylor, J. R., "Nanosecond pulsed 620 nm source by frequency-doubling a phosphosilicate Raman fiber amplifier," *Optics Letters* **44**(24), 6025–6028 (2019).

[32] Rulkov, A. B., Popov, S. V., and Taylor, J. R., "1.5-2 µm, multi-Watt white-light generation in CW format in highly-nonlinear fibres," in [*Advanced Solid-State Photonics*], *Advanced Solid-State Photonics* , TuA6, OSA Technical Digest, Optical Society of America (2004).